Influence of Y₂O₃-SiC-Mo and Ce-Al-Ni amorphous alloy on laser melting deposition stellite matrix composites

Jia-Ning Li[1]*, Hai-Long Ma[1], Ai-Jun Tang[1,2], Xing-Dong Yuan[1], Yu-Shuang Huo[1]

[1]*School of Materials Science and Engineering, Shandong Jianzhu University, Jinan 250101, P. R. China*
[2]*College of Mechanical and Electronic Engineering, Shandong Jianzhu University, Jinan 250101, P. R. China*

Abstract

Nanostructured catalytic powders (NCP) were used to produce the laser melting deposition (LMD) amorphous-nanocrystalline composite coatings on titanium alloy. With amorphous alloy addition, amorphous surrounded nanoscale polycrystals (ASNP) and amorphous surrounded one-dimensional nanocrystals (ASON) were produced. A composite coating was fabricated by LMD of the Stellite 6-TiB₂ mixed powders on a TA15 alloy. Scanning Electron Microscope (SEM) test results indicated that with Y_2O_3-SiC-Mo addition, an LMD amorphous-nanocrystalline composite coating was obtained. The addition of the Ce-Al-Ni amorphous alloy led a micro-nano structure LMD coating to be produced. This research provided essential theoretical and experimental basis to promote the application of LMD technique in the modern aviation industry.

1. Introduction

LMD as a new production route plays an important role in the field of an aviation industry. LMD is a rapid forming technology for building metallic components. The laser deposited metal parts have a fine microstructure, and mechanical properties of the laser deposited parts are usually comparable or even superior to the forged materials [1, 2]. In the last decade, the nanocomposites have become very popular because of their high toughness and stiffness along with superior hardness. Nanocomposites differ from the conventional composites due to the particularly high surface-to-volume ratio of ceramic reinforcement [3–6]. Amorphous materials have also attracted an increasing amount of attention due to their unique physical, mechanical and chemical properties [7–10]. LMD is a promising approach to producing the amorphous-nanocrystalline composites on metals. In the past few years, the efforts were mainly focused on the mechanical properties of LMD coarse structure coatings [11, 12], while less work has been carried out on LMD amorphous-nanocrystalline composites, especially using NCP to fabricate this kind of composites on met-als. Such object matter is the research focus of this study.

LMD Stellite 6-TiB₂ pre-placed powders on a TA15 titanium alloy can produce the coarse, hard composites. Through experimental work, it was confirmed that with the addition of Y_2O_3-SiC-Mo, an amorphous-nanocrystalline composite coating was obtained on a TA15 substrate; moreover, with Ce-Al-Ni amorphous powder addition, an interesting phenomenon occurred: ASNP and ASON were produced. In this study, the influence of the Y_2O_3-SiC-Mo powders and Ce-Al-Ni amorphous alloy on LMD Stellite 6 matrix composites was investigated in detail.

2. Experimental

Materials used in this experiment: TA15 samples, size of 10 mm × 10 mm × 10 mm, were abraded with abrasive paper prior to the coating operation. Chemical compositions (wt.%) of TA15: 6.06Al, 2.08Mo, 1.32V, 1.86Zr, 0.09Fe, 0.08Si, 0.05C, 0.07O and bal. Ti. Pre-placed powders of Stellite 6 (≥ 99.5 % purity, 20–100 μm), TiB₂ (≥ 99.5 % purity, 2–50 μm), SiC

Table 1. The materials of LMD in experiment

Number	Powders composition (wt.%)
Sample 1	80Stellite 6-20TiB_2
Sample 2	73Stellite 6-20TiB_2-1Y_2O_3-3.5SiC-2.5Mo
Sample 3	70.5Stellite 6-20TiB_2-1Y_2O_3-3.5SiC-2.5Mo-2.5(Ce-Al-Ni)

($\geq$ 99.5 % purity, 10–50 μm), Mo ($\geq$ 99.5 % purity, 10–40 μm), and Y_2O_3 ($\geq$ 99.5 % purity, 2–20 μm) were used for LMD. Chemical compositions (wt.%) of Stellite 6: 1.20C, 29.00Cr, 1.50Si, 1.50Mo, 1.00Mn, 1.00Fe, 3.00W, 3.00Ni, 1.00B and bal. Co. Ce-Al-Ni amorphous powder ($\geq$ 99.5 % purity, 10–50 μm) was also used as the laser melting powder, and its chemical compositions (wt.%): 68.00Ce, 17.00Al, 15.00Ni.

Melting powders were pre-placed on the surface of substrates using a water glass ($Na_2O \cdot nSiO_2$), to form a layer of 0.8 mm thickness. A cross-flow laser (TRUMPF, Ditzingen, Germany) was employed to melt the surface of three samples, and argon gas at a pressure of 0.4 MPa was fed through a nozzle that was coaxial with the laser beam. Process parameters of laser melting: laser power $P = 1.0$ kW, scanning velocity $V = 3$–7.5 mm s^{-1}, and the laser beam diameter $D = 4$ mm. An overlap of 35 % between successive tracks was selected. Parameters of all samples were the same during LMD process, and the materials in the experiment are shown in Table 1.

Metallographic samples were prepared using standard mechanical polishing procedures and then etched in a solution of HF, HNO_3, and H_2O in a volume ratio of 1:1:4 to reveal the growth morphologies of compounds in such LMD composites. Microstructural morphologies of such composites were analyzed by means of a QUANTA200 SEM (FEI, Amsterdam, Holland) and a JEM-2100 high-resolution transmission electron microscope (HRTEM) (JEOL, Osaka, Japan). Phase constitutions were determined by X-ray diffraction (XRD) using a D/MAX-RC equipment (Rigaku Corporation, Osaka, Japan). Elements distributions of the composites were measured using an E/DAXGenesis2000 (FEI, Amsterdam, Holland) energy dispersive spectrometer (EDS). An HV-1000 micro sclerometer (Shanghai Zhongyan Instrument Manufacturing plant, Shanghai, P.R. China) was used to measure the microhardness distribution of the composites.

3. Results and analysis

As shown in Fig. 1a, a metallurgical combination was obtained between the LMD composite coating and TA15 substrate in sample 1. The matrix phase was a solid solution of Ni and Co with some B, Cr, Si,

and Fe, etc., providing a dendritic structure; there was an interdendritic lamellar eutectic phase, which mainly consisted of Ni and Co, and also small amounts of B and Si, etc. It was noticed that the coarse stick/block-shape precipitates were dispersed in the cell-shape coating matrix (see Fig. 1b). As shown in Fig. 1c, a fine and compact microstructure is obtained in bottom-coating of sample 2; lots of the nanoscale particles and nanorods were produced in such coating (see Fig. 1d). It was considered that Y_2O_3-SiC-Mo led the coarse precipitates to decompose during an LMD process.

As shown in Fig. 2a, lots of nanoscale particles were produced in the composite coating of sample 2. Obviously, Y_2O_3-SiC-Mo played an important role in refining the microstructure of LMD coating. On the other hand, the production of nanoscale particles is also ascribed to the sufficiently rapid heating and cooling of an LMD technique. Moreover, during LMD process, a little Y was released from the pre-placed coating, which refined the microstructures, also improved the strength and ductility of such coating [13]. The addition of the proper SiC-Mo content also played an effective role in refining the microstructures of such composites. Investigations [14, 15] indicate that SiC is an effective grain refiner for laser-treated coatings due to its high melting point. Mo compounds, such as $Mo_5(Si,Al)_3C$ were produced through the in situ metallurgical reaction during laser melting process, which also refined the microstructures of laser-treated coatings. TiB_2 crystal structure is the alternating series of the hexagonal symmetrical titanium and boride layers, and its cylinder index is {1010} . (0001) plane is vertical to a cylindrical surface, and its growth direction is along the (1010) lateral plane. It is known that TiB_2 crystals do not include the crystal plane and the direction of obvious growth advantage, favoring to the formations of the block-shape precipitates [16]. Furthermore, due to the sufficiently rapid cooling rate of laser molten pool, TiB_2 did not have enough time to grow up, leading to the formation of the nanocrystals (see Fig. 2b). It was noted that TiB nanorods were also produced in the coating of sample 2 (see Fig. 2c). In fact, due to the dilution effect, lots of Ti entered into the molten pool from the substrate, favoring to formations of the TiB one-dimensional nanoscale precipitates [17].

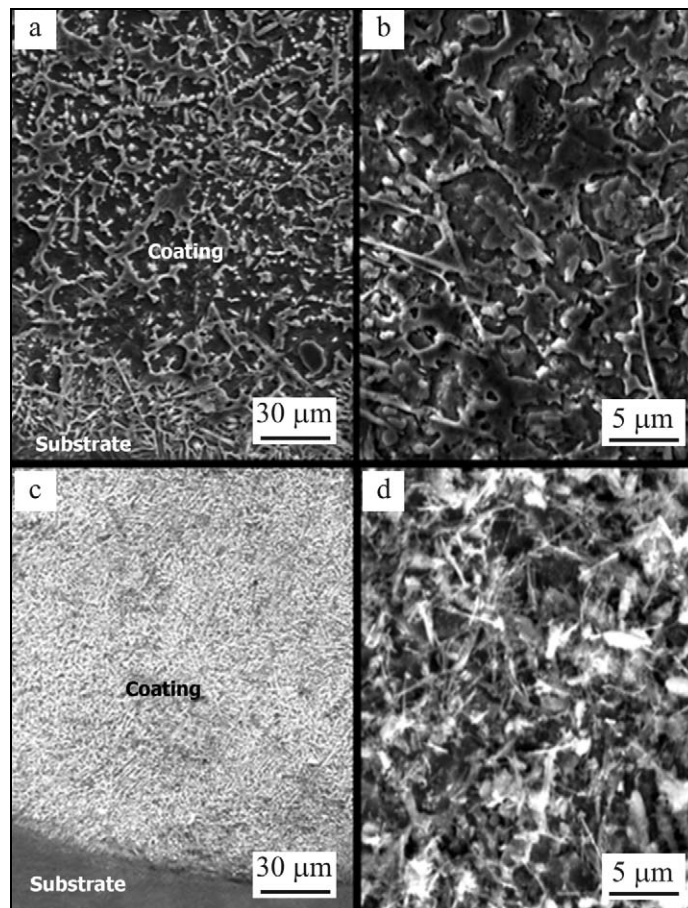During LMD process, lots of Si, Fe and Zr entered

Fig. 1. SEM micrographs of the coatings in samples 1 (a, b), and 2 (c, d).
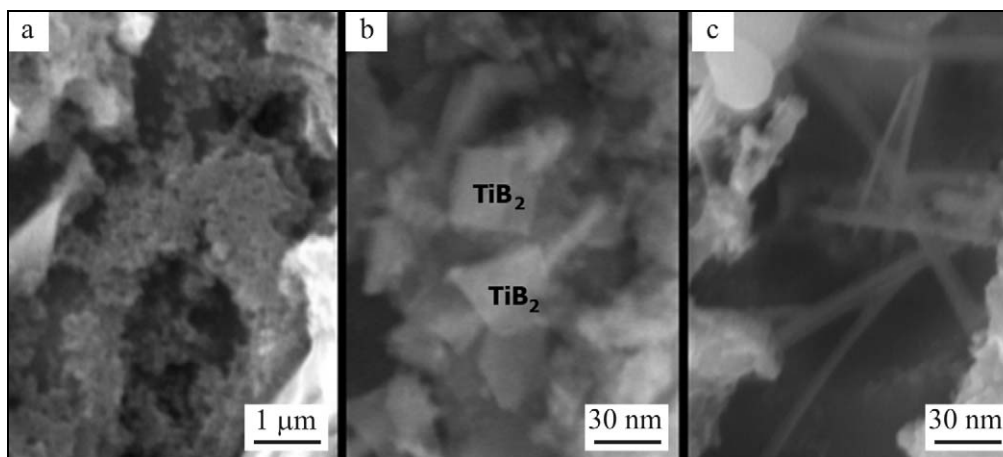

Fig. 2. SEM and TEM micrographs of the coating in sample 2: (a) SEM micrographs of the nanoscale particles; (b) TiB_2 nanocrystals; (c) TiB one-dimensional nanocrystals.

into the molten pool from the substrate. It is known that a series of amorphous alloys have high glass forming ability in Si, Fe, Zr and Y based alloy systems [18–21]. Thus, it was speculated that a lot of amorphous phases were able to be produced in such LMD coating.

As shown in Fig. 3a, with Ce-Al-Ni amorphous powder addition, the micro-nano particles were ob-

tained in the coating of sample 3. HRTEM irregular lattice of the selected particle was observed, indicating that such particle mainly consisted of the amorphous phases (see Fig. 3b). Thus, it was speculated that during the solidification process of laser molten pool, Ce-Al-Ni alloy softened, then precipitated around the nanocrystals, leading to the forma-
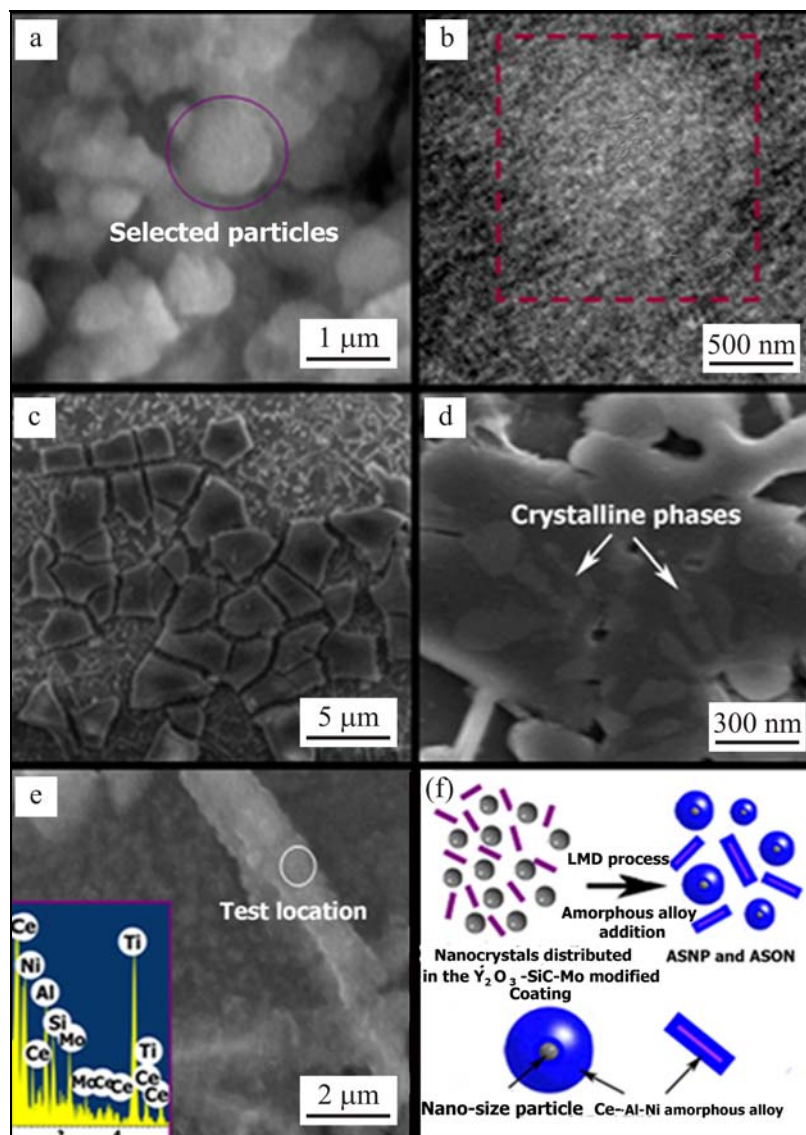
Fig. 3. SEM micrograph of ASNP (a), and its HRTEM image (b); SEM micrographs of the large amorphous blocks (c, d); SEM micrograph of ASON and its corresponding EDS spectrum (e); schematic diagram of the ASNP and ASON formation processes (f).

tion of a coarse structure. This kind of particles was ASNP. As shown in Fig. 3c, lots of large amorphous blocks were produced in the coating of sample 3; the crystalline phases were included in such amorphous blocks (see Fig. 3d). The EDS test was performed in the location of stick-shape precipitates, the result indicating that the Al, Ti, Ni, Mo and Ce diffraction peaks were present in the EDS spectrum (see Fig. 3e). It was known that added amorphous powders mainly consisted of Ce, Al, and Ni. Thus, according to the EDS spectrum, it was located that Ce-Al-Ni amorphous alloy was included in the stick-shape precipitate; moreover, the diffraction peaks of Ti and Mo were also present in the EDS spectrum. In fact, the electron probe was possible to explore the chemical compositions of the coating matrix, so the diffraction

peaks of Ti and Mo were also present. The EDS image indicated that ASON was produced in the coating of sample 3. The schematic diagram of the ASNP and ASON formation process is shown in Fig. 3f.

As shown in Fig. 4a, the microhardness distribution of LMD coating in sample 2 was in the range of 1400–1550 $HV_{0.2}$, which was approximately 3 times higher than that of the substrate (about 390 $HV_{0.2}$), an enhancement of microhardness of such coating was mainly ascribed to the fine and compact microstructure and the phase constituent. The microhardness distribution of the coating in sample 3 was in a range of 1400–1550 $HV_{0.2}$, which was very similar to that of the coating in sample 2. It was considered that though added amorphous alloy coarsened the microstructure of coating, the amorphous alloy showed the high hard-
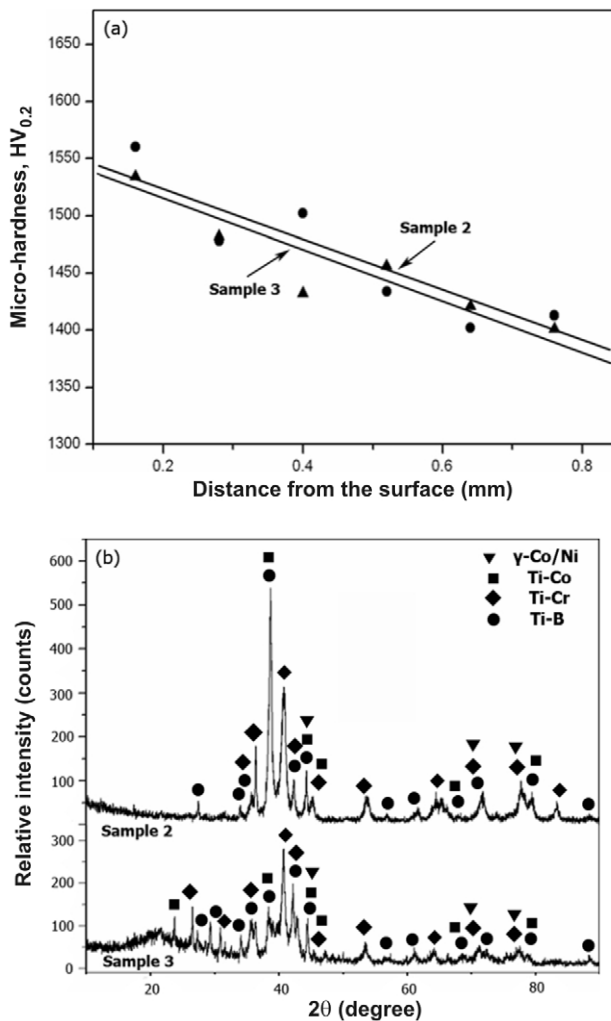
Fig. 4. Microhardness distributions of the coatings in samples 2 and 3 (a); XRD diagram of the coatings in samples 2 and 3 (b).

ness, favoring an enhancement of microhardness.

As shown in Fig. 4b, X-ray diffraction patterns indicated that the composite coatings in samples 2 and 3 consisted mainly of γ-Co/Ni, Ti-Co, Ti-Cr intermetallics, and Ti-B compounds, and these compounds were produced through the in situ metallurgical reactions, which could be attributed to a high energy density of the laser beam. Due to the low content of other compounds, such as SiC, Y_2O_3, and TiAl, etc., their diffraction peaks were not produced obviously in XRD diagram. It was noted that with an amorphous powder addition, the broad diffraction peaks appeared at $2\theta = 15°–35°$ and $38°–45°$ are present, indicating that added amorphous powders played an important amorphization effect on the LMD composite coatings.

4. Conclusions

In summary, LMD of the Stellite 6-TiB_2 pre-placed

powders on TA15 substrate can form a hard coating, which exhibited a coarse structure. With Y_2O_3-SiC--Mo addition, an amorphous-nanocrystalline composite coating was obtained. Y_2O_3-SiC-Mo addition led the coarse precipitates to decompose after an LMD process, leading to the formations of nanoscale particles and nanorods. Such composite coating mainly consisted of the amorphous phases, the Ti-Ni, Ti-Cr intermetallics and Ti-B compounds. Due to a rapid solidification process of molten pool, a portion of the amorphous phases just began to crystallize when the laser molten pool had completed the solidification process. With the addition of the Ce-Al-Ni amorphous alloy, lots of micro/nano size ASNP were produced, leading to the formation of a micro-nano structure LMD coating. Added amorphous powder also played an important amorphization effect on the LMD composite coatings.

References

[1] Liu, D., Zhang, S. Q., Li, A., Wang, H. M.: J. Alloys Compd., *485*, 2009, p. 156. doi:10.1016/j.jallcom.2009.05.112
[2] Qu, H. P., Wang, H. M.: Mater. Sci. Eng. A, *466*, 2007, p. 187. doi:10.1016/j.msea.2007.02.073
[3] Gu, D. D., Hagedorn, Y., Meiners, W., Wissenbach, K., Poprawe, R.: Compos. Sci. Technol., *71*, 2011, p. 1612. doi:10.1016/j.compscitech.2011.07.010
[4] Gu, D. D., Meng, G. B., Li, C., Meiners, W., Poprawe, R.: Scripta Mater., *67*, 2012, p. 185. doi:10.1016/j.scriptamat.2012.04.013
[5] Li, K., Chai, B., Peng, T. Y., Mao, J., Zan, L.: ACS Catalysis, *3*, 2013, p. 170. doi:10.1021/cs300724r
[6] Vijayan, B. K., Dimitrijevic, N. M., Finkelstein-Shapiro, D., Wu, J. S., Gray, K. A.: ACS Catalysis, *2*, 2012, p. 223. doi:10.1021/cs200541a
[7] Li, J. N., Yu, H. J., Chen, C. Z., Gong, S. L.: J. Phys. Chem. C, *117*, 2013, p. 4568. doi:10.1021/jp311138f
[8] Wang, J. W., Liu, X. H., Zhao, K. J., Palmer, A., Patten, E., Burton, D., Mao, S. X., Suo, Z. G., Huang, J. Y.: ACS Nano, *6*, 2012, p. 9158. doi:10.1021/nn3034343
[9] Zhu, Z. H., Ma, J. Q., Xu, L., Xu, L., Li, H. X.: ACS Catalysis, *2*, 2012, p. 2119. doi:10.1021/cs300472p
[10] Matthews, D. T. A., Ocelik, V., Branagan, D., de Hosson, J. T. M.: Surf. Coat. Technol., *203*, 2009, p. 1833. doi:10.1016/j.surfcoat.2009.01.015
[11] Wang, Y. D., Tang, H. B., Fang, Y. L., Wang, H. M.: Mater. Sci. Eng. A, *528*, 2010, p. 474. doi:10.1016/j.msea.2010.09.038
[12] Chen, L. Q., Chan-Park, M. B., Zhang, Q., Chen, P., Li, C. M., Li, S.: Small, *5*, 2009, p. 1043. doi:10.1002/smll.200801210

[13] Tian, Y. S., Chen, C. Z., Chen, L. X., Huo, Q. H.: Scripta Mater., *54*, 2006, p. 847. doi:10.1016/j.scriptamat.2005.11.011

[14] Li, W., Shan, S. F., Fang, Q. H.: Surf. Eng., *28*, 2012, p. 594. doi:10.1179/1743294412Y.0000000036

[15] Lusquińos, F., Pou, J., Quintero, F., Pérez-Amor, M.: Surf. Coat. Technol., *202*, 2008, p. 1588. doi:10.1016/j.surfcoat.2007.07.011

[16] Tian, Y. S., Zhang, Q. Y., Wang, D. Y., Chen, C. Z.: Cryst. Growth Des., *8*, 2008, p. 700. doi:10.1021/cg0608099

[17] Li, J. N., Chen, C. Z., He, Q. S.: Mater. Chem. Phys., *133*, 2012, p. 741. doi:10.1016/j.matchemphys.2012.01.082

[18] Wang, J. W., Liu, X. H., Zhao, K. J.: ACS Nano, *6*, 2012, p. 9158. doi:10.1021/nn3034343

[19] McMillan, P. F.: Nature Mater., *3*, 2004, p. 755. doi:10.1038/nmat1248

[20] Sotiriou, G. A., Franco, D., Poulikakos, D.: ACS Nano, *6*, 2012, p. 3888. doi:0.1021/nn205035p

[21] Zhang, J. Y., Liu, G., Lei, S. Y., Niu, J. J., Sun, J.: Acta Mater., *60*, 2012, p. 7183. doi:10.1016/j.actamat.2012.09.027